Molecular Electronic Level Alignment at Weakly Coupled Organic Film/Metal Interfaces

Jin Zhao,[*,†,‡,§] Min Feng,[‡] Daniel Barker Dougherty,[⊥] Hao Sun,[†] and Hrvoje Petek[†,‡]

[†]Department of Physics and ICQD/Hefei National Laboratory for Physical Sciences at Microscale, and [§]Synergetic Innovation Center of Quantum Information & Quantum Physics, University of Science and Technology of China, Hefei, Anhui 230026, P. R. China, [‡]Department of Physics and Astronomy, University of Pittsburgh, Pittsburgh, Pennsylvania 15260, United States, and [⊥]Department of Physics, North Carolina State University, Raleigh, North Carolina 27695, United States

ABSTRACT Electronic level alignment at interfaces of molecular materials with inorganic semiconductors and metals controls many interfacial phenomena. How the intrinsic properties of the interacting systems define the electronic structure of their interface remains one of the most important problems in molecular electronics and nanotechnology that can be solved through a combination of surface science experimental techniques and theoretical modeling. In this article, we address this fundamental problem through experimental and computational studies of molecular electronic level alignment of thin films of C_6F_6 on noble metal surfaces. The unoccupied electronic structure of C_6F_6 is characterized with single molecule resolution using low-temperature scanning tunneling microscopy-based constant-current distance-voltage spectroscopy. The experiments are performed on several noble metal surfaces with different work functions and distinct surface-normal projected band structures. In parallel, the electronic structures of the quantum wells (QWs) formed by the lowest unoccupied molecular orbital state of the C_6F_6 monolayer and multilayer films and their alignment with respect to the vacuum level of the metallic substrates are calculated by solving the Schrödinger equation for a semiempirical one-dimensional (1D) potential of the combined system using input from density functional theory. Our analysis shows that the level alignment for C_6F_6 molecules bound through weak van der Waals interactions to noble metal surfaces is primarily defined by the image potential of metal, the electron affinity of the molecule, and the molecule surface distance. We expect the same factors to determine the interfacial electronic structure for a broad range of molecule/metal interfaces.

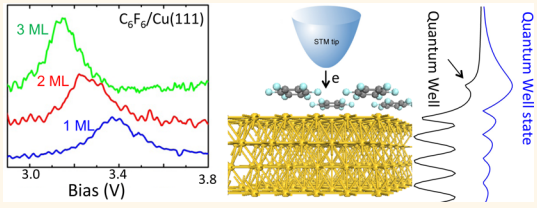

KEYWORDS: energy level alignment · image potential · quantum well state

Molecular materials have enormous potential for applications in electronics and nanotechnology. The emerging applications of molecule-based electronics require a fundamental knowledge of how the intrinsic properties of molecules and substrates define their interfacial electronic structure.[1−8] Although there are several experimental and theoretical methods, which could be applied to study the interfacial electronic structure for such systems, to predict the electronic properties at molecular/metal interfaces by a simple method, which only requires the knowledge of the noninteracting components, for example like the Mott−Schottky[9,10] model for the band alignment at semiconductor interfaces, would greatly advance our ability to design novel molecule-based electronic devices.[11] Sophisticated interfacial band structure calculations based on the many-body perturbation theory,[12,13] which give an accurate description of the interfacial screening, have been proven to give near-quantitative agreement with experiment.[14,15] These methods, however, remain highly computationally demanding and costly, constraining their applications in many practical systems of interest, such as in photocatalysis and photovoltaics.[16,17]

Hexafluorobenzene (C_6F_6) molecular quantum wells (QWs) present an intriguing model for molecular semiconductors because they form interfaces with metal substrates through weak dispersion forces, and unusually, their lowest unoccupied molecular (LUMO) orbitals on account of their σ^* symmetry undergo intermolecular hybridization into a strongly dispersive conduction band (CB).[18] The unoccupied electronic structure of highly ordered thin C_6F_6 films adsorbed on Cu(111) surfaces was first studied using two-photon photoemission (2PP) spectroscopy by Zhu, Wolf, and

* Address correspondence to zhaojin@ustc.edu.cn, petek@pitt.edu.

Received for review September 4, 2014 and accepted October 6, 2014.

Published online October 06, 2014
10.1021/nn5049969

co-workers.[19−25] Unlike their aromatic hydrocarbon counterparts, C_6F_6 films grow in layered planar structures from the monolayer to multilayer films.[18] For a C_6F_6 monolayer (ML) on a Cu(111) surface they found a sharp resonance at 3.14 eV above the Fermi level (E_F), which they attributed to the LUMO state-derived quantum well that forms the molecular CB. Energy, momentum, and coverage-dependent measurements of the CB revealed nearly free electron (NFE) dispersion corresponding to an effective mass of $2m_e$ (m_e is the free electron mass) at 1 ML coverage; increasing the layer thickness to 5 ML further enhanced the intermolecular interactions, decreasing both the band mass to $1m_e$ and the band minimum to 2.84 eV.[22] Concomitantly with completing 1 ML coverage, the $n = 1$ image potential (IP) state of the bare Cu(111) surface disappeared, and no corresponding IP state of the C_6F_6 overlayer was found. Gahl *et al*. attributed the NFE properties of the CB and disappearance of the IP state to strong hybridization between them: in their model, the NFE properties were not intrinsic to C_6F_6, but rather were imparted by strong interaction between the IP state and LUMO of C_6F_6 causing the strong downshift of the resulting hybrid state.[22]

Subsequently, we reexamined the NFE band formation by the σ^* state of C_6F_6 using single-molecule resolved scanning tunneling microscopy (STM) and first-principles calculations.[18] These studies revealed the superatom character of the σ^* state wave function,[26,27] which has non-nuclear probability density maxima. The wave function penetration beyond the F atom periphery enables a strong intermolecular wave function overlap imparting the NFE properties to C_6F_6 QWs even without molecule−surface interaction. The diffuse nature of the σ^* orbital, originally found in DFT calculations, was recently elaborated by the equation-of-motion method.[28] The role of the metal substrate, and in particular the IP potential, in defining the electronic structure at the C_6F_6 QW/metal interface, however, remains unclear.

In this article, we elaborate the interfacial electronic structure of C_6F_6 thin films on different metal surfaces by combined STM and electronic structure theory methods. We perform low-temperature STM and scanning tunneling spectroscopy (STS) experiments on C_6F_6 thin films with 0−3 ML coverage adsorbed on four noble metal surfaces, Cu(111), Cu(110), Au(111), and Au(100), which present a variety of work functions and surface-projected band structures. These measurements provide the molecular layer thickness and metal substrate-dependent information about the unoccupied electronic structure of noble metal−supported C_6F_6 QWs.

The experimental data are simulated by a theoretical approach that has been shown to describe quantitatively the electronic structure of alkali-atom−noble-metal interfaces.[11,29] To overcome the shortcomings of DFT, namely underestimation of the quasiparticle band gap and failure to reproduce the long-range image potential, we extend the semiempirical approach for describing the surface electronic structure of metals of Chulkov and co-workers to account for the modification by molecular adsorbates.[30] The Chulkov potentials for different surfaces are parametrized to reproduce the surface electronic structure (Shockley and image potential surface states) as well as the bulk projected band gaps within the s,p-conduction bands of typical metals. They include the universal $1/4z$ dependence of the image potentials of metals, in which z is the distance from the image plane.[11,30−32] DFT calculations including dispersion forces provide the adsorption structures of the C_6F_6 molecules. The surface electronic structure is calculated by adding the perturbing adsorbate pseudopotential to the substrate Chulkov potential and solving the resulting 1D Schrödinger equation for the combined system. Our analysis indicates that for C_6F_6 films on metal surfaces, the image potential is the decisive factor in determining the interfacial electronic level alignment. Nevertheless, the IP states of the combined system, which penetrate into the CB of C_6F_6, are strongly perturbed and lose their identity by interaction with the molecular overlayer. We expect the same approach for calculating the interfacial electronic structure to be broadly applicable to other weakly coupled molecule−metal systems.

RESULTS AND DISCUSSION

STM Measurements of C_6F_6 QWs on Different Noble Metal Surfaces. Figure 1 gives the low temperature STM measurements of the molecular and electronic structure of C_6F_6 QWs adsorbed on Cu(111), Au(111), Au(100), and Cu(110) surfaces. Figure 1a shows an STM image of the Cu(111) surface with bare regions and C_6F_6 islands with 1−3 ML thickness. The first monolayer has a unit cell with a lateral dimension of 0.74 ± 0.02 nm, in agreement with the (3 × 3) superlattice structure observed by low energy electron diffraction, as well at the real space STM images.[22] The next two layers have essentially identical real-space structures with molecules of subsequent layers aligning with the hollow sites of the previous layer in an ABAB··· stacking. The planar stacking in the first three layers contrasts with the previously observed structure of thin films of benzene on Cu surfaces,[33] where a herringbone structure emerges in the second and higher MLs. The planar stacking imaged by STM for 1−3 ML in Figure 1 is consistent with NEXAFS studies, which show it to persist for at least 10 C_6F_6 layers on Cu(111).[34] C_6F_6 thin film structures on Au(100)-(5 × 20) and Au(111)-(22 × $\sqrt{3}$) reconstructed surfaces are almost identical to the structure on Cu(111) [Figure 1 panels b and c, top row]. On Au(100) and Au(111) surfaces the molecular layer heights are modulated by the underlying metal surface reconstructions.[35,36] The rectangular unit cell

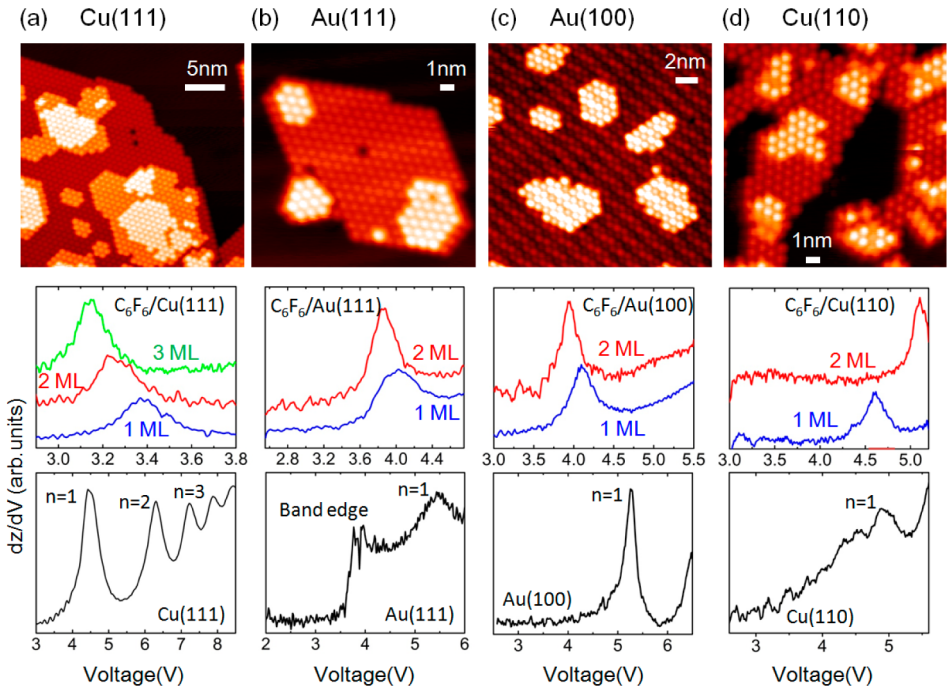

Figure 1. STM images and dz/d*V* spectra of C_6F_6 covered (a) Cu(111); (b) Au(111); (c) Au(100); and (d) Cu(110) surfaces. The spectra are taken on the bare metal regions (bottom row) and 1−3 ML thick molecular quantum wells. The imaging conditions for C_6F_6 multilayers are 9 pA current and 1.5 V bias voltage. The d//d*V* measurements are recorded at a constant current of 9 pA.

dimensions of Cu(110) combined with the preferred hexagonal tiling of C_6F_6 molecules cause extended molecular vacancy defects to appear at irregular intervals within the ordered C_6F_6 overlayers [Figure 1d, top]. Such defects were also observed for the benzene monolayer on Cu(110).[33,37]

The dz/d*V* spectra measured locally on areas of the surface with C_6F_6 thicknesses from 0 to 3 ML reveal the electronic structure of the bare surfaces and C_6F_6 QWs (Figure 1, middle and bottom row). As in 2PP spectra,[19,22] the IP states of the bare surface and resonance peak associated with the σ^* LUMO of C_6F_6 QWs are observed. The new findings are (i) the observed resonance energy strongly depends on the metal substrate, and (ii) for Cu(111), Au(111), and Au(100) surfaces, the observed resonance energy decreases with the increasing thickness, whereas for the Cu(110) surface, the opposite occurs.

The resonances in dz/d*V* spectra of the clean and C_6F_6 covered surfaces are at a higher energy by a fraction of an eV than the corresponding states in the 2PP spectra, where the data are available. This systematic deviation between the two spectroscopic methods has been attributed to a Stark shift induced by the STM tip in dz/d*V* spectra.[37−39] We verified that at the measurement current of 9 pA there is no current-dependent Stark shift, only an offset from the 2PP resonance energies. These offsets are not caused by the tip morphology as judged by the better than 20 meV reproducibilities of the resonance energies. Table 1 presents the observed Stark shifts for IP states obtained in ref 38. Similar Stark shifts are also present in dz/d*V* measurements of C_6F_6 QW energies, but are only known for the Cu(111) substrate. From the comparison between our dz/d*V* energies with the previous 2PP measurements in ref 22 on Cu(111), we find a Stark shift of 0.25 eV, which is comparable with 0.33 eV for the n = 1 IP state reported in ref 38. Because there are no corresponding 2PP results available for the other metal surfaces, we use the Stark shift values for IP states from ref 38 to correct the QW energies found in the STM measurements.

TABLE 1. Stark Shift of the dz/d*V* Spectroscopic Features Representing the Difference between the Observed Energies of the n = 1 IP States from 2PP and STM Measurements Presented in Reference 38

	Cu(111)	Au(111)	Au(100)	Cu(110)
n = 1 (eV) (STM)	4.44	5.55	5.18	4.98
n = 1 (eV) (2PP)	4.11	4.89	4.84	4.00
Stark shift (eV)	0.33	0.66	0.34	1.0

Electronic Structure of C_6F_6 on Cu(111), Au(111) and Au(100) Surfaces. The electronic structure of C_6F_6 on Cu(111), Au(111), and Au(100), as determined from dz/d*V* spectra, can be easily understood from their corresponding 1D model potentials by solving for the eigenvalues. Figure 2a presents the 1D model potential of 1 ML C_6F_6 on a Cu(111) surface, in which $z = 0$ is set to the position of an image plane of a bare surface.[30] The position of the QW center, that is, the adsorption distance (Z_{ads}) of C_6F_6 from the image plane of Cu(111) obtained from

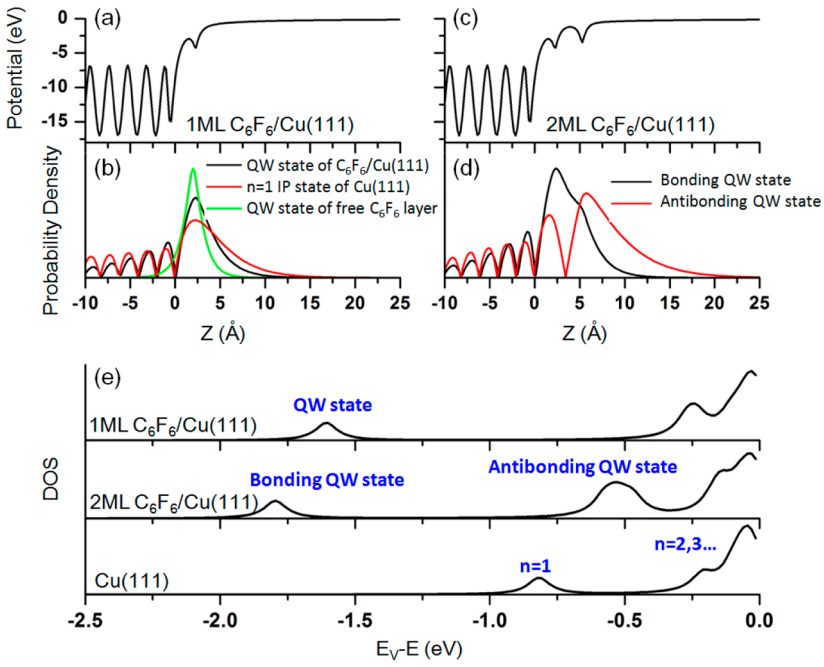

Figure 2. (a and c) The 1D potentials for one and two molecule thick QWs of C_6F_6 on a Cu(111) surface. (b) The probability densities for a free C_6F_6 QW, the $n = 1$ IP state of clean Cu(111) surface, and the 1 ML thick C_6F_6 QW on a Cu(111) surface for the potential in panel a. (d) The probability densities of the bonding and antibonding states of 2 ML thick C_6F_6 QW on a Cu(111) surface for the potential in panel c. (e) The densities of states (DOS) of the clean Cu(111) surface, as well as 1 and 2 ML C_6F_6 QWs on a Cu(111) surface calculated from the 1D potentials, such as in Figure 1 panels a and c.

DFT-D calculations, which include the van der Waals interaction through a semiempirical dispersion potential, is 1.96 Å. The eigenstates of the potential obtained by solving the 1D Schrödinger equation give the first QW state at −1.6 eV with respect to the vacuum level (E_v). According to the STM results, the C_6F_6 resonance peak in Figure 1a is 3.35 eV above E_F. If we subtract a Stark shift of 0.33 eV (Table 1) and use 4.63 eV for the work function of C_6F_6/Cu(111),[25] then the STM measurement implies a binding energy of −1.61 eV, in good agreement with the 1D model potential calculation. The QW energies obtained by 1D model potential, STM measurements, and 2PP measurements are summarized in Table 2.

The 1D wave function of the QW state is plotted in Figure 2b together with the unsupported QW state and the $n = 1$ IP state of the bare Cu(111) surface. The QW state wave function obtained by solving the Schrödinger equation shows that it is primarily bound to the QW, but that it also penetrates into the surface and has image potential character. On one hand, the wave function has the largest probability localized in the QW, maintaining the character of the QW state of the isolated monolayer. On the other hand, the wave function also has some characteristics of the image potential state having similar penetration into the surface, maximum amplitude at approximately the same distance from the image plane, and a tail extending into the vacuum. In this sense, the electronic properties of the QW at the interface can be understood in terms of penetration of the $n = 1$ IP state of the

TABLE 2. Calculated Z_{ads} and the QW State Energies with Respect to E_F from STM Measurements, 2PP Spectra, and 1D Model Potential Calculation

		Cu(111)	Au(111)	Au(100)	Cu(110)
Z_{ads} (Å)	1 ML (DFT)	1.97	2.02	2.24	2.11
E_{QW} (eV)	1 ML (STM)	3.04	3.27	3.75	
	1 ML (model)	3.03	3.30	3.79	
	1 ML (2PP)	3.15			
	1 ML (DFT)	2.0	2.6	1.5	2.2
	2 ML (STM)	2.88	3.09	3.55	
	2 ML (model)	2.84	3.12	3.57	
	2 ML (2PP)	2.97			
	3 ML (STM)	2.76			
	3 ML (model)	2.72			
	3 ML (2PP)	2.90			
E_{IP} (eV)	1 ML (STM)				3.6
	1 ML (model)				4.0
	2 ML (STM)				4.1
	2 ML (model)				4.2

Cu(111) surface into the CB of the C_6F_6 QW state. This is consistent with the weak sensitivity of the energy and lifetime of the C_6F_6 QW state to adsorption of an insulating Xe overlayer on top of C_6F_6 molecular films, which strongly perturbs conventional IP states.[22] Furthermore, there is no additional state distinct from the QW state that is a solution of the 1D potential, which could be assigned to the $n = 1$ IP state, as reported in 2PP studies.[25] The Schrödinger equation allows for the $n > 1$ solutions converging the vacuum level, which both penetrate into the QW state and extend into the vacuum. These states do not appear prominently in

either the STM and 2PP measurements, except for the case of Cu(110), which we will discuss in more detail.

The resonance energy downshift of 2 ML C_6F_6 on Cu(111) can also be explained by using a two-layer QW to describe the system, as shown in Figure 2c). The second C_6F_6 layer is located at 0.31 nm above the first according to the DFT-D calculations. For the 2 ML case, the QW supports two states with eigenenergies of −1.79 and −0.66 eV corresponding to a bonding and antibonding interaction pair. As for the 1 ML QW, only the lowest energy bonding state appears prominently in the d*z*/d*V* spectra; its energy downshift by 0.19 eV agrees with the d*z*/d*V* and 2PP spectra.[22] In Figure 2e the density of states (DOS) of Cu(111) and 1 and 2 ML of C_6F_6 on Cu(111) are plotted. Using the same method, the QW states of 3 ML C_6F_6 could be obtained. The resonance energy downshift of the bonding QW state is in good agreement with the STM measurements after subtracting the Stark shift (Table 2).

The electronic structure of C_6F_6 on Au(111) and Au(100) could also be interpreted as for Cu(111), using a QW potential for C_6F_6 plus the corresponding Chulkov's model potentials for the substrates.[30] To compare with the experimental binding energy of the lowest QW state, we need to estimate the work functions of Au(111) and Au(100) with C_6F_6 adsorption. We note that the work function decrease of C_6F_6 on Cu(111) is 0.32 eV,[25] which is induced by the Pauli repulsion between the metal surface and adsorbate charge densities resulting in charge redistribution.[40] Because the interaction of C_6F_6 with different metal surfaces is quite similar, and no independent experimental measurements are available, we use the same work function decrease for all the metal surfaces discussed in this report. On the basis of this assumption, the calculated QW states resonance energies are in good agreement with the STM measurements as shown in Table 2.

One can see that the binding energy of the QW state is the highest on the Au(111) surface and lowest for the Au(100) surface. This could be understood from an additional interaction, namely the electronic hybridization repulsion between the QW state and the Shockley surface state on (111) surfaces of noble metals, which stabilizes the Shockley and destabilizes the QW state. Because the surface state energies of Au(111), Cu(111), and Au(100) are at −6.05, −5.52, and −3.87 eV with respect to E_v, respectively, the repulsion between the QW state with the surface is the strongest for the Au(100) surface since the energy difference between the surface state [in the case of Au(100) it is a resonance] and the QW state is the smallest. For the same reason, the repulsion between the most deeply bound Shockley surface state and QW state is weakest for the Au(111) surface. These additional substrates have different work functions, intrinsic surface state energies, and projected band gaps, which are captured by the Chulkov potential, and therefore it is expected that such details would be reflected in the calculated properties of the QW state.

Electronic Structure of C_6F_6 on the Cu(110) Surface. The electronic structure of C_6F_6 on the Cu(110) surface shows distinct behavior from the other surfaces. The two significant differences between Cu(110) and the other three surfaces are first, the resonance energies are higher, and consequently the binding energies are lower, than for the other surfaces; and second, counterintuitively the resonance energy increases instead of decreasing on going from 1 to 2 ML C_6F_6 QW.

These distinct characteristics could be due to the C_6F_6 QWs being resonant with the bulk continuum of Cu(110) at the Γ point, whereas for the other surfaces the QWs exist within a projected band gap [Cu(111) and Au(100)] or at the band edge of the bulk bands [Au(111)]. To simulate this surface, a jellium model including the image potential is used as shown in Figure 3a,c. The strong broadening exceeding 1 eV of the QW DOS seen in Figure 3e is a consequence of their hybridization with the resonant bulk bands.

In the case of strong resonant broadening due to the coupling with a continuum, the surface electronic structure subject to the resonant scattering should be described by the resonance trapping model, which was discussed in ref 41. According to Höfer and co-workers, in the case of a single surface localized state coupling with a bulk continuum, the level simply broadens with the increasing coupling.[41] If the potential, however, supports two or more states, a more complex outcome ensues. Interpreting 2PP spectra of the strongly coupled image potential states of the prototypical jellium metal, Al(100), Höfer and co-workers found that the $n = 1$ resonance DOS is suppressed and its density is distributed among higher states, whereas the $n \geq 2$ IP resonances appear with narrower line widths than would be expected by considering the coupling of each state individually.[41] In the resonance coupling model, the coupling between the discrete state and the continuum is transferred to the lowest state of the series, as evidenced by its broadening, and suppressed for the higher order states.

The same physics appears to be also affecting the surface electronic structure of C_6F_6 QWs on Cu(110). The jellium model calculation in Figure 3e indicates a large broadening of QW states, which increases with the number of C_6F_6 monolayers, whereas the higher order IP states above them remain relatively narrow, and their widths decrease. The qualitative difference in the coupling of the QW states and the higher order IP states can also be seen in the wave function penetration into the substrate in Figure 3b,d. The increased coupling of both the bonding state and the antibonding state for 2 ML C_6F_6 with the bulk continuum increases the width of the QW DOS and pushes the high order IP states to higher energy, consistent with the resonance trapping model. Table 2 gives the

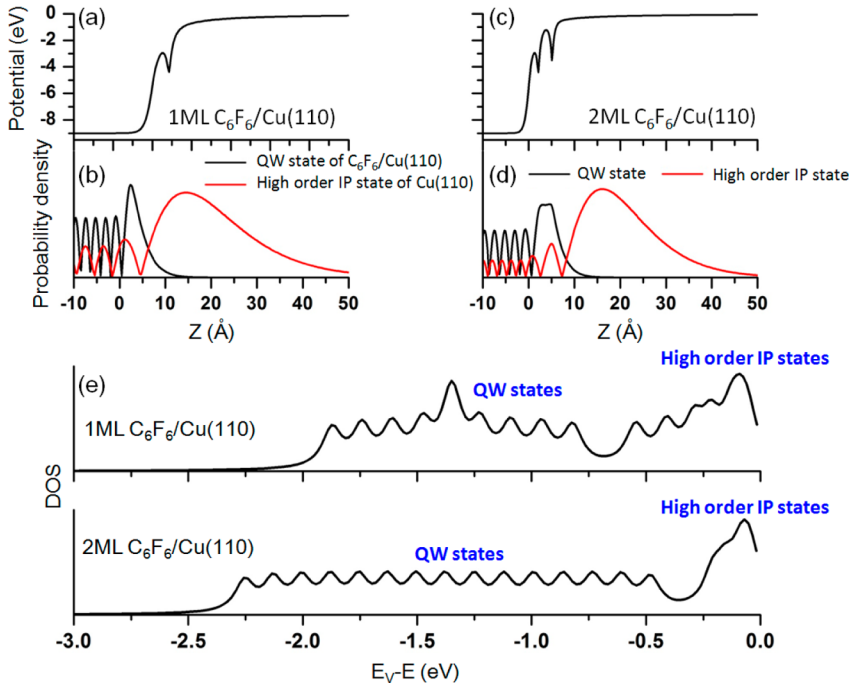

Figure 3. (a and c) The 1D potentials for one and two molecule thick QWs of C_6F_6 on a Cu(110) surface. (b) The probability densities of high order IP states of a clean Cu(110) surface, and the 1 ML thick C_6F_6 QW on a Cu(110) surface for the potential in panel a. (d) The probability densities of the QW states and high order IP states of 2 ML thick C_6F_6 QW on a Cu(110) surface for the potential in panel b. (e) The densities of states (DOS) of 1 and 2 ML C_6F_6 QWs on a Cu(110) surface calculated from the 1D potentials, such as in Figure 2a,b.

energies of the high order IP states obtained by the model potential, which agree well with the behavior of the observed resonance in the STM measurements on C_6F_6/Cu(110) films, if the experimentally observed resonance is attributed to them rather than the QW states. Thus, we conclude that the exceptional behavior of C_6F_6/Cu(110) surfaces can be attributed to extreme broadening of the QW state, which is not observed in d*I*/d*V* measurements, and the accompanying upshift of the higher order IP states, which appear as a resonance in the absence of the QW state.

It is interesting to contrast our observations for the unoccupied electronic structure of C_6F_6 on Cu(110) with the case of benzoate adsorption on the same surface.[42] For benzoate adsorbed in an upright geometry on Cu(110) a very sharp n = 1 image potential state was observed whose response to the local molecular environment could be captured within an effective dielectric continuum model. Unlike C_6F_6, benzoate is not a strong electron acceptor and an intrinsic molecular quantum well would not form. When combined with spatial wave function decoupling due to the upright adsorption geometry, this leads to a weaker coupling to the Cu(110) bulk continuum states and thus avoids the resonance trapping that suppresses the $n = 1$ state for C_6F_6 adsorbates.

Universal Image Potential Effects on Quantum Well States. Although the resonance energy of the C_6F_6 QW state depends on the properties of the surface support, our analysis shows that the most important property of a metal that determines the resonance energy is the universal image potential. The image potential is included in our model potentials, but is missing from theoretical methods that do not include the long-range exchange-correlation interaction, such as most forms of DFT.[32] In Figure 4a we plot the QW state energy dependence on the Z_{ads} measured from the image plane of Cu(111), Au(111), and Au(100) surfaces that we investigated. When Z_{ads} is infinite, that is, for single layer C_6F_6, the QW state energy is that of the free monolayer; that is, $E_A = -0.39$ eV.[18,28] As the C_6F_6 QW approaches the surface, the QW state energy initially decreases following the same $1/4z$ dependence as the image potential. In the absence of other interactions, the C_6F_6 QW state energy would follow the universal $E_A - 1/4z$ curve, also shown in Figure 4a, for every surface. When the distance is smaller than around 6 Å, the QW state starts to hybridize with the surface and bulk states of the substrate; thereupon their binding energies with respect to E_v start to deviate from the $E_A - 1/4z$ curve. The interaction with the substrate is predominantly repulsive causing the QW state to be pushed above the $E_A - 1/4z$ curve through the hybridization with surface states and resonances.[43]

The Z_{ads} for the three surfaces in Figure 4a varies from 1.97 to 2.24 Å, as indicated by the circles. In the case of physisorption Z_{ads} is determined by a balance of van der Waals attraction and Pauli repulsion.[11] At these distances the most significant electronic interaction, which stabilizes the QW state energy by more

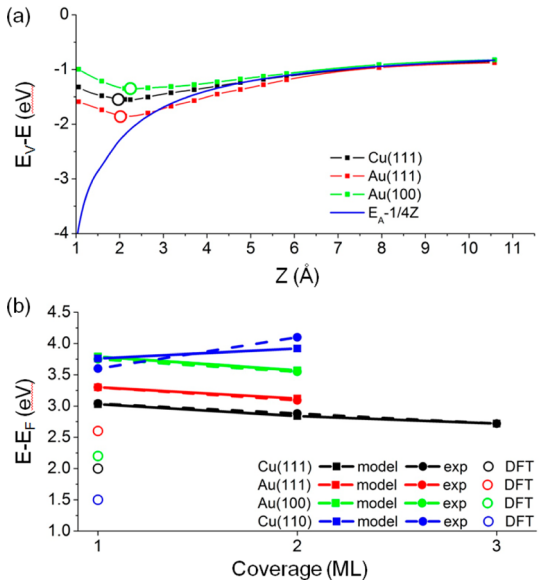

Figure 4. (a) The dependence of 1 ML thick QW state binding energy on the distance between the molecular and the image planes for the metal Cu(111), Au(111), and Au(100) surfaces. The $E_A-1/4z$ curve represents the universal behavior of the QW state binding energy in the absence of hybridization-induced level repulsion. (b) The resonance energies with respect to the E_F obtained by STM, 1D model potential and DFT for 1 and 2 ML of C_6F_6 adsorbed on different metal surfaces. The solid and dashed lines connect the binding energy of different coverage C_6F_6 obtained by model potential and STM experiments.

than −2 eV, is still the image charge attraction. Therefore, the differences from the $E_A-1/4z$ curve to the calculated binding energies of −1.85 to −1.35 eV at the Z_{ads} represent the hybridization-induced state repulsion.

The universal electronic structure of C_6F_6 on different metals is anticipated in our studies of the electronic structure of alkali atoms on metal surfaces.[11,29] In the case of alkali atoms, one electron is transferred to the metal in the chemisorbed state, forming essentially a pure ionic bond with the substrate.[44] The energy level alignment of alkali atom LUMO, which is populated to form the neutral alkali atom adsorbate, is determined by the Coulomb interaction of the valence electron with its own image charge and that of the positive ion core. In the case of C_6F_6 physisorption, the charge transfer is negligible and its LUMO has anionic character. The LUMO energy level alignment is defined by the image charge interaction of the anionic LUMO with the metal surface. Our results clearly show that if the electronic states of the anion formed by localizing an electron in the LUMO of the adsorbate, rather than having it shared with the surface in a covalent bond, then the electronic level alignment mostly depends on the image charge effects.

Our model confirms the crucial role of image charge effects for the molecular orbital energy level alignment of weakly coupled molecules on metals. The dominant image potential, however, is frequently not included, for example, in DFT calculations. In Figure 4b we have plotted the energy of the 1 ML C_6F_6 conduction band minimum for the four metal surfaces obtained by DFT calculations using the PBE functional, together with the results obtained by model potential and STM experiments. One can see that the DFT results show large deviation most likely due to the well-known underestimation of the quasiparticle band gap,[45] in addition to the exclusion of the image potential. Higher level first-principles calculations for example within the GW approximation are able to predict the molecular electronic levels at solid−molecule interfaces, though their computational cost is much higher.[12,13] Yet the results of GW calculations also show that as long as LUMO and HOMO are localized on the adsorbate, their energy alignment follows the $1/4z$ trend of image potential, in agreement with our much simpler approach. In the case that HOMO and LUMO are delocalized, DFT level theory results can be corrected provided one accounts for the anisotropic screening at the molecule/metal interface.[14,15]

Failures of the Model. One prediction of our model, which is not fully confirmed by the STM experiments, is the existence of the antibonding state for 2 ML quantum wells. Figure 2e suggests that such a state should exist ∼1 eV above the bonding state, but it is has not been identified in our experiments. Gahl *et al.* report an additional peak ∼0.4 eV above the bonding state in 2PP spectra to C_6F_6 QWs with 3−5 ML thickness, which they attributed to a higher order QW state.[33] This feature is hardly observable in 2PP spectra of 3 ML owing to its large width and short lifetime compared with the bonding state. Considering the low signal level in 2PP spectra, we assume that such higher order states make insufficient contribution to the tunneling probability to be observed as distinct resonances in the dz/dV spectra. In fact, we can only see the higher-order states in the case of the Cu(110) surface, when the primary bonding state is too broad to detect because of its coupling with the bulk continuum. Thus, it is likely that the higher-order states exist, but their contributions are obscured by the intense bonding state in the dz/dV spectra.

Other Semiempirical Models. In a significant body of literature on molecular electronics, it is assumed that the frontier level alignment is determined by the interfacial dipole, and the consequent work function change, that occurs when a molecular overlayer is brought into contact with a substrate.[46,47] The interface dipole effect is a consequence of adsorption induced charge transfer, and thus depends on the type of molecule−surface interactions, for example, chemisorption vs physisorption, as well as direction of the charge flow. The image charge effect always stabilizes the frontier orbitals of adsorbates by a magnitude that depends on the molecular distance from the image plane, and can easily exceed −2 eV for typical

physisorption distances. In the case of C_6F_6 QWs on a Cu(111) surface, 2PP measurements give the work function change due to the interface dipole only −0.3 eV, whereas the image charge and hybridization shifts for the Au and Cu surfaces, which are reported in Figure 4, exceed −1 eV. Polarization effects are also important on semiconductor surfaces, but are not as pronounced as on metals.[16] Therefore, the relative importance of the interface dipole versus image charge effects also depends on the nature of the substrate.

Another approach to the calculation of the interfacial electronic structure is the dielectric continuum model (DCM),[48,49] which was applied by Gahl *et al*. to interpretation of C_6F_6 QW electronic structure for 1−5 ML coverage.[33] They considered DCM to give an unsatisfactory account of the coverage dependence of the C_6F_6 QW state energies, because it could not reproduce the higher order states. The failure of the DCM model, however, could have been in part due to the incorrect assumption that the second and higher monolayers of C_6F_6 adopt the upright structure of benzene bilayer and multilayers.[33] Moreover, DCM models the electronic properties of the overlayer with a dielectric constant and electron affinity, which are uniform throughout the overlayer, and thus do not represent the physical situation accurately. The description of the C_6F_6 overlayers in the present model with theoretically motivated pseudopotentials provides a more realistic description of the metal−molecule interface and thus is expected to be more successful than the DCM approach.

CONCLUSIONS

Using STM measurements and 1D model potential, we have investigated the electronic level alignment of C_6F_6 on different metal surfaces. The alignment of C_6F_6 QW LUMO on different metal surfaces observed by dz/d*V* spectroscopy using STM could be explained using a 1D model potential including the binding of C_6F_6 QW and 1D semiempirical potential to describe the image charge effects and the electronic hybridization with the surface and bulk bands of the metal substrate. Our study reveals that for weakly coupled molecular/metal systems, image potential and the molecular electron affinity play the dominant roles in determining the electronic level alignment at the molecule/metal interface. The properties of the substrate, such as the work function and Pauli repulsion from the surface charge density, also have important roles, which can produce significant substrate dependence of the unoccupied state binding energy. We expect our study to provide valuable insights into the design of molecule/metal interfaces with desired electronic properties.

METHODS

The STM measurements are performed at ∼5K under ultrahigh vacuum conditions. Because C_6F_6 is relatively weakly bound on metals,[21] tunneling spectroscopy in constant height current−voltage mode is not feasible; tip-induced motion or reaction prevent measurements at large tip−sample biases required to probe the CB of C_6F_6. To perform electronic spectroscopy, therefore, we adopt the constant current distance−voltage, *z*(*V*) mode. In this measurement, the constant current feedback loop is engaged while the tip−sample bias is increased; to maintain a small tunneling current the tip retracts from the surface. The tip displacement *z* is measured as a function of tip−sample bias *V*; the signature of resonant tunneling appears in abrupt displacement of the tip as the voltage is scanned through surface resonances. This spectroscopic mode has been successfully applied to studies of electronic structures of bare and molecule-covered surfaces at bias voltages approaching and even exceeding the vacuum level.[18,50,51]

The metal substrate surfaces are prepared within a preparation chamber by standard surface science techniques and transferred through a gate valve to the STM measurement chamber. C_6F_6 molecules purified by several freeze−pump−thaw cycles are dosed onto the metal substrates at surface temperatures between 10 and 100 K within the STM chamber. STM images are measured with electrochemically etched tungsten tips. For distance−voltage measurements, the STM tip is positioned above the approximate center of molecular features. All dz/d*V* spectra presented in this work are the average of several *z*(*V*) measurements on either different molecules or different points on the bare substrate; the averaged measurements are subsequently numerically differentiated to identify the tunneling resonances.

The theoretical investigations are carried out by a combination of first-principles and model potential calculations. The adsorption structures are obtained from DFT calculations including dispersion interactions. Plane-wave basis set DFT electronic structure calculations with a cutoff energy of 400 eV using the generalized gradient approximation are performed with the PBE functional[52] as implemented in the Vienna *ab initio* simulation package (VASP).[53−55] The projector augmented wave method describes the electron−ion interaction.[56] The surfaces are represented with a six-layer metal atom slab with C_6F_6 placed on one side including the dipole moment correction and 1.5 nm thick vacuum. The C_6F_6 adsorption on Cu(111), Cu(110), and Au(111) surfaces is modeled with one molecule per substrate (3 × 3) unit cell, whereas for Au(100) a (2 × 2) unit cell is adopted. To account for the dispersion interaction, the structures are calculated with the DFT-D approach adding a semiempirical dispersion potential to the Kohn−Sham DFT energy.[57]

The surface electronic structure of C_6F_6 overlayers is described by a 1D quantum well (QW) model potential. Modeling the surface electronic structure of C_6F_6 layers with a 1D surface-normal QW potential is appropriate because of the NFE properties of the molecular LUMO. The fully screened potential, therefore, varies only in the *z* direction as

$$V = A_{10} + A_1 \cos(\beta|z| + \pi) \quad |z| < z_1 - \frac{\pi}{\beta} \tag{1}$$

$$V = A_2 \exp\left[-\alpha\left(|z| + \frac{\pi}{\beta} - z_1\right)\right] \quad |z| > z_1 - \frac{\pi}{\beta} \tag{2}$$

Equations 1 and 2 contain six parameters: $A_{10}, A_1, \beta, z_1, A_2, \alpha$, but only three are independent because the potential and its first derivative are required to be continuous. We chose $A_{10} = -1.8$, $A_1 = 1.0$ and $\beta = 4.0$ to fit the model potential, where A_{10}, A_1, and β determine the depth and the width of the QW. The QW parameters are adjusted until the potential reproduces the electron affinity (E_A) of unsupported 1 ML C_6F_6, which is

determined by the E_A of a single molecule (0.135 eV)[28] plus the energy stabilization associated with the intermolecular band formation (0.25 eV);[18] the double QW of an unsupported molecular bilayer has an energy splitting between the bonding and antibonding states of 0.8 eV, which is close to 0.9 eV given by the plane wave DFT calculations.

The Cu(111), Au(111), and Au(100) surfaces are described by 1D potentials developed by Chulkov *et al.*[30] to reproduce the respective projected band gaps and the surface states. To reproduce the image potential states, the Chulkov potential includes the long-range image potential, which has the $1/4z$ dependence beyond the image plane.[31] The Cu(110) surface does not have a projected band gap at the Γ point, and therefore, we simulate it using the jellium model. Because DFT calculations show that C_6F_6 molecules interact with the metal surfaces mainly through the dispersion forces and the charge transfer between them is negligible, we build the 1D model potential for the C_6F_6/metal interface by adding the metal and QW potentials with the molecular plane located relative to the metal surface plane according to the adsorption height given by the DFT-D calculations. Finally, solving the Schrödinger equation gives the binding energies and 1D wave functions of the bound states.

Conflict of Interest: The authors declare no competing financial interest.

Acknowledgment. The authors thank J. T. Yates, Jr. for encouragement and support. The STM instrumentation used in the experiments was purchased with support form the W. M. Keck Foundation. The authors acknowledge DOE-BES Division of Chemical Sciences, Geosciences, and Biosciences Grant No. DE-FG02-09ER16056, for the research conducted at the University of Pittsburgh, and National Science Foundation of China Grants No. NSFC21121003, 11322434, and the Fundamental Research Funds for the Central Universities WK2340000034 for the research conducted at the University of Science and Technology of China. Some calculations were performed at the Shanghai supercomputer center and Environmental Molecular Sciences Laboratory at the PNNL, a user facility sponsored by the DOE Office of Biological and Environmental Research.

REFERENCES AND NOTES

1. Tautz, F. S. Structure and Bonding of Large Aromatic Molecules on Noble Metal Surfaces: The Example of PTCDA. *Prog. Surf. Sci.* **2007**, *82*, 479–520.
2. Koch, N. Energy Levels at Interfaces between Metals and Conjugated Organic Molecules. *J. Phys.: Condens. Matter* **2008**, 184008.
3. Petek, H.; Feng, M.; Zhao, J. The Electronic Structure of Metal–Molecule Interfaces. In *Current-Driven Phenomena in Nanoelectronics*; Seideman, T., Ed.; World Scientific: Singapore, 2010.
4. Han, P.; Weiss, P. S. Electronic Substrate-Mediated Interactions. *Surf. Sci. Rep.* **2012**, *67*, 19–81.
5. Jia, C.; Guo, X. Molecule-Electrode Interfaces in Molecular Electronic Devices. *Chem. Soc. Rev.* **2013**, *42*, 5642–5660.
6. Coropceanu, V.; Li, H.; Winget, P.; Zhu, L.; Brédas, J.-L. Electronic-Structure Theory of Organic Semiconductors: Charge-Transport Parameters and Metal/Organic Interfaces. *Annu. Rev. Mater. Res.* **2013**, *43*, 63–87.
7. Koitaya, T.; Mukai, K.; Yoshimoto, S.; Yoshinobu, J. Energy Level Alignment of Cyclohexane on Rh(111) Surfaces: The Importance of Interfacial Dipole and Final-State Screening. *J. Chem. Phys.* **2013**, *138*, 044742.
8. Marks, M.; Schöll, A.; Höfer, U. Formation of Metal–Organic Interface States Studied with 2PPE. *J. Electron Spectrosc. Relat. Phenom.* **2014**, *195*, 263–271.
9. Mott, N. F. The Contact between a Metal and an Insulator or Semiconductor. *Proc. Cambridge Philos. Soc.* **1938**, *34*, 568–572.
10. Schottky, W. Simplified and Extended Theory of Barrier-Layer Rectifiers. *Z. Phys.* **1942**, *118*, 539–592.
11. Zhao, J.; Pontius, N.; Winkelmann, A.; Sametoglu, V.; Kubo, A.; Borisov, A. G.; Sanchez-Portal, D.; Silkin, V. M.; Chulkov, E. V.; Echenique, P. M.; Petek, H. Electronic Potential of a Chemisorption Interface. *Phys. Rev. B* **2008**, *78*, 085419.
12. Neaton, J. B.; Hybertsen, M. S.; Louie, S. G. Renormalization of Molecular Electronic Levels at Metal–Molecule Interfaces. *Phys. Rev. Lett.* **2006**, *97*, 216405.
13. Thygesen, K. S.; Rubio, A. Renormalization of Molecular Quasiparticle Levels at Metal–Molecule Interfaces: Trends across Binding Regimes. *Phys. Rev. Lett.* **2009**, *102*, 046802.
14. Migani, A.; Mowbray, D. J.; Iacomino, A.; Zhao, J.; Petek, H.; Rubio, A. Level Alignment of a Prototypical Photocatalytic System: Methanol on TiO_2(110). *J. Am. Chem. Soc.* **2013**, *135*, 11429–11432.
15. Migani, A.; Mowbray, D. J.; Zhao, J.; Petek, H.; Rubio, A. Quasiparticle Level Alignment for Photocatalytic Interfaces. *J. Chem. Theory Comput.* **2014**, *10*, 2103–2113.
16. Garcia-Lastra, J. M.; Rostgaard, C.; Rubio, A.; Thygesen, K. S. Polarization-Induced Renormalization of Molecular Levels at Metallic and Semiconducting Surfaces. *Phys. Rev. B* **2009**, *80*, 245427.
17. Marom, N.; Körzdörfer, T.; Ren, X.; Tkatchenko, A.; Chelikowsky, J. R. Size Effects in the Interface Level Alignment of Dye-Sensitized TiO_2 Clusters. *J. Phys. Chem. Lett.* **2014**, *5*, 2395–2401.
18. Dougherty, D. B.; Feng, M.; Petek, H.; Yates, J. T., Jr.; Zhao, J. Band Formation in a Molecular Quantum Well *via* 2D Superatom Orbital Interactions. *Phys. Rev. Lett.* **2012**, *109*, 266802.
19. Vondrak, T.; Zhu, X. Y. Two-Photon Photoemission Study of Heterogeneous Electron Transfer: C_6F_6 on Cu(111). *J. Phys. Chem. B* **1999**, *103*, 3449–3456.
20. Ishioka, K.; Gahl, C.; Wolf, M. Femtosecond Dynamics of Image Potential States of C_6F_6/Cu(111) Studied with Two-Photon Photoemission. *Surf. Sci.* **2000**, *454–456*, 73–77.
21. Zhu, X.-Y.; Vondrak, T.; Wang, H.; Gahl, C.; Ishioka, K.; Wolf, M. Photo-Induced Electron Transfer to Molecular Quantum Structures on a Metal Surface. *Surf. Sci.* **2000**, *451*, 244–249.
22. Gahl, C.; Ishioka, K.; Zhong, Q.; Hotzel, A.; Wolf, M. Structure and Dynamics of Excited Electronic States at the Adsorbate/Metal Interface: C_6F_6/Cu(111). *Faraday Discuss.* **2000**, *117*, 191–202.
23. Dutton, G.; Zhu, X. Y. Electronic Band Formation at Organic–Metal Interfaces: Role of Adsorbate–Surface Interaction. *J. Phys. Chem. B* **2001**, *105*, 10912–10917.
24. Zhu, X.-Y. Electron Transfer at Molecule–Metal Interfaces: A Two-Photon Photoemission Study. *Annu. Rev. Phys. Chem.* **2002**, *53*, 221–247.
25. Kirchmann, P. S.; Loukakos, P. A.; Bovensiepen, U.; Wolf, M. Ultrafast Electron Dynamics Studied with Time-Resolved Two-Photon Photoemission: Intra- and Interband Scattering in C_6F_6/Cu(111). *New J. Phys.* **2005**, *7*, 113–128.
26. Feng, M.; Zhao, J.; Petek, H. Atomlike, Hollow-Core-Bound Molecular Orbitals of C_{60}. *Science* **2008**, *320*, 359–362.
27. Feng, M.; Zhao, J.; Huang, T.; Zhu, X.-Y.; Petek, H. The Electronic Properties of Superatom States of Hollow Molecules. *Acc. Chem. Res.* **2011**, *44*, 360–368.
28. Voora, V. K.; Jordan, K. D. Nonvalence Correlation-Bound Anion State of C_6F_6: Doorway to Low-Energy Electron Capture. *J. Phys. Chem. A* **2013**, *118*, 7201–7205.
29. Wang, L.-M.; Sametoglu, V.; Winkelmann, A.; Zhao, J.; Petek, H. Two-Photon Photoemission Study of the Coverage-Dependent Electronic Structure of Chemisorbed Alkali Atoms on a Ag(111) Surface. *J. Phys. Chem. A* **2011**, *115*, 9479–9484.
30. Chulkov, E. V.; Silkin, V. M.; Echenique, P. M. Image Potential States on Metal Surfaces: Binding Energies and Wave Functions. *Surf. Sci.* **1999**, *437*, 330–352.
31. Echenique, P. M.; Pendry, J. B. Theory of Image States at Metal Surfaces. *Prog. Surf. Sci.* **1990**, *32*, 111–172.
32. Constantin, L. A.; Pitarke, J. M. Adiabatic-Connection-Fluctuation-Dissipation Approach to Long-Range Behavior of Exchange-Correlation Energy at Metal Surfaces: A Numerical Study for Jellium Slabs. *Phys. Rev. B* **2011**, *83*, 075116.

33. Lee, J.; Dougherty, D. B.; Yates, J. T., Jr. Edge-on Bonding of Benzene Molecules in the Second Adsorbed Layer on Cu(110). *J. Phys. Chem. B* **2006**, *110*, 15645–15649.
34. Vijayalakshmi, S.; Föhlisch, A.; Kirchmann, P. S.; Hennies, F.; Pietzsch, A.; Nagasono, M.; Wurth, W. Bond Polarization and Image-Potential Screening in Adsorbed C_6F_6 on Cu-(111). *Surf. Sci.* **2006**, *600*, 4972–4977.
35. Binnig, G. K.; Rohrer, H.; Gerber, C.; Stoll, E. Real-Space Observation of the Reconstruction of Au(100). *Surf. Sci.* **1984**, *144*, 321–335.
36. Barth, J. V.; Brune, H.; Ertl, G.; Behm, R. J. Scanning Tunneling Microscopy Observations on the Reconstructed Au-(111) Surface—Atomic-Structure, Long-Range Superstructure, Rotational Domains, and Surface-Defects. *Phys. Rev. B* **1990**, *42*, 9307–9318.
37. Dougherty, D. B.; Maksymovych, P.; Lee, J.; Yates, J. T., Jr. Stark-Shifted Image Potential States of Benzene Bilayers on Cu(110) and Cu(111). *Chem. Phys. Lett.* **2006**, *431*, 303–307.
38. Dougherty, D. B.; Maksymovych, P.; Lee, J.; Feng, M.; Petek, H.; Yates, J. T., Jr. Tunneling Spectroscopy of Stark-Shifted Image Potential States on Cu and Au Surfaces. *Phys. Rev. B* **2007**, *76*, 125428.
39. Pronschinske, A.; Mardit, D. J.; Dougherty, D. B. Modeling the Constant-Current Distance−Voltage Mode of Scanning Tunneling Spectroscopy. *Phys. Rev. B* **2011**, *84*, 205427.
40. Witte, G.; Lukas, S.; Bagus, P. S.; Wöll, C. Vacuum Level Alignment at Organic/Metal Junctions: "Cushion" Effect and the Interface Dipole. *Appl. Phys. Lett.* **2005**, *87*, 263502.
41. Winter, M.; Chulkov, E. V.; Höfer, U. Trapping of Image-Potential Resonances on a Free-Electron-like Surface. *Phys. Rev. Lett.* **2011**, *107*, 236801.
42. Pronschinske, A.; Dougherty, D. B. Impact of Local Molecular Environment on the Decay of Image Potential States. *J. Phys. Chem. Lett.* **2010**, *1*, 2613–2617.
43. Galbraith, M. C. E.; Marks, M.; Tonner, R.; Höfer, U. Formation of an Organic/Metal Interface State from a Shockley Resonance. *J. Phys. Chem. Lett.* **2013**, *5*, 50–55.
44. Trioni, M. I.; Achilli, S.; Chulkov, E. V. Key Ingredients of the Alkali Atom—Metal Surface Interaction: Chemical Bonding versus Spectral Properties. *Prog. Surf. Sci.* **2013**, *88*, 160–170.
45. Hybertsen, M. S.; Louie, S. G. Electron Correlation in Semiconductors and Insulators: Band Gaps and Quasiparticle Energies. *Phys. Rev. B* **1986**, *34*, 5390–5413.
46. Ishii, H.; Sugiyama, K.; Ito, E.; Seki, K. Energy Level Alignment and Interfacial Electronic Structures at Organic/Metal and Organic/Organic Interfaces. *Adv. Mater.* **1999**, *11*, 605–625.
47. Zhu, X. Y. Electronic Structure and Electron Dynamics at Molecule−Metal Interfaces: Implications for Molecule-Based Electronics. *Surf. Sci. Rep.* **2004**, *56*, 1–82.
48. Cole, M. W. Electronic Surface States of a Dielectric Film on a Metal Substrate. *Phys. Rev. B* **1971**, *3*, 4418–4422.
49. Wong, C. M.; McNeill, J. D.; Gaffney, K. J.; Ge, N. H.; Miller, A. D.; Liu, S. H.; Harris, C. B. Femtosecond Studies of Electron Dynamics at Dielectric−Metal Interfaces. *J. Phys. Chem. B* **1999**, *103*, 282–292.
50. Alvarado, S. F.; Seidler, P. F.; Lidzey, D. G.; Bradley, D. D. C. Direct Determination of Exciton Binding Energy of Conjugated Polymers Using a Scanning Tunneling Microscope. *Phys. Rev. Lett.* **1998**, *81*, 1082–1085.
51. Pascual, J. I.; Corriol, C.; Ceballos, G.; Aldazabal, I.; Rust, H. P.; Horn, K.; Pitarke, J. M.; Echenique, P. M.; Arnau, A. Role of the Electric Field in Surface Electron Dynamics above the Vacuum Level. *Phys. Rev. B* **2007**, *75*, 165326.
52. Perdew, J. P.; Burke, K.; Ernzerhof, M. Generalized Gradient Approximation Made Simple. *Phys. Rev. Lett.* **1996**, *77*, 3865–3868.
53. Kresse, G.; Hafner, J. *Ab Initio* Molecular Dynamics for Liquid Metals. *Phys. Rev. B* **1993**, *47*, 558–561.
54. Kresse, G.; Hafner, J. *Ab initio* Molecular Dynamics for Open-Shell Transition Metals. *Phys. Rev. B* **1993**, *48*, 13115.
55. Kresse, G.; Hafner, J. *Ab-Initio* Molecular-Dynamics Simulation of the Liquid−Metal Amorphous-Semiconductor Transition in Germanium. *Phys. Rev. B* **1994**, *49*, 14251–14269.
56. Kresse, G.; Joubert, D. From Ultrasoft Pseudopotentials to the Projector Augmented-Wave Method. *Phys. Rev. B* **1999**, *59*, 1758–1775.
57. Wu, X.; Vargas, M. C.; Nayak, S.; Lotrich, V.; Scoles, G. Towards Extending the Applicability of Density Functional Theory to Weakly Bound Systems. *J. Chem. Phys.* **2001**, *115*, 8748–8757.